

Structural Analysis of Phospholipase A₂ from Functional Perspective. 1. Functionally Relevant Solution Structure and Roles of the Hydrogen-Bonding Network^{†,‡}

Chunhua Yuan,[§] In-Ja L. Byeon,^{||} Yishan Li,[⊥] and Ming-Daw Tsai^{*,§,||,⊥,#}

Departments of Chemistry and Biochemistry, Campus Chemical Instrument Center, and Ohio State Biochemistry Program, The Ohio State University, Columbus, Ohio 43210

Received September 14, 1998; Revised Manuscript Received December 17, 1998

ABSTRACT: Bovine pancreatic phospholipase A₂ (PLA2), a small (13.8 kDa) Ca²⁺-dependent lipolytic enzyme, is rich in functional and structural character. In an effort to examine its detailed structure–function relationship, we determined its solution structure by multidimensional nuclear magnetic resonance (NMR) spectroscopy at a functionally relevant pH. An ensemble of 20 structures generated has an average root-mean-square deviation (RMSD) of 0.62 ± 0.08 Å for backbone (N, C^α, C) atoms and 0.98 ± 0.09 Å for all heavy atoms. The overall structure shows several notable differences from the crystal structure: the first three residues at the N-terminus, the calcium-binding loop (Y25–T36), and the surface loop (V63–N72) appear to be flexible; the α-helical conformation of helix B (E17–F22) is absent; helix D appears to be shorter (D59–V63 instead of D59–D66); and the hydrogen-bonding network is less defined. These differences were analyzed in relation to the function of PLA2. We then further examined the H-bonding network, because its functional role or even its existence in solution has been in dispute recently. Our results show that part of the H-bonding network (the portion away from N-terminus) clearly exists in solution, as evidenced by direct observation (at 11.1 ppm) of a strong H-bond between Y73 and D99 and an implicated interaction between D99 and H48. Analyses of a series of mutants indicated that the existence of the Y73•••D99 H-bond correlates directly with the conformational stability of the mutant. Loss of this H-bond results in a loss of 2–3 kcal/mol in the conformational stability of PLA2. The unequivocal identification and demonstration of the structural importance of a specific hydrogen bond, and the magnitude of its contribution to conformational stability, are uncommon to the best of our knowledge. Our results also suggest that, while the D99•••H48 catalytic diad is the key catalytic machinery of PLA2, it also helps to maintain conformational integrity.

Mammalian pancreatic phospholipase A₂ (PLA2,¹ EC 3.1.1.4), part of the growing PLA2 super family (1, 2), are calcium-dependent lipolytic enzymes. The enzymes are

typically small (13~15 kDa) and highly homologous. They have been studied extensively for their structure, function, and catalytic mechanism. Our contributions to this field have been published in the “Phospholipase A₂ Engineering” series (3). The system used in our studies is PLA2 from bovine pancreas overexpressed in *Escherichia coli* (13.8 kDa, 123 amino acids). While we have used proton NMR extensively in these studies, the focus has been mainly on the functional side, and the NMR analysis was largely qualitative.

[†] This work was supported by NIH Grant GM 41788 to M.-D.T. The study made use of a Bruker DMX-600 NMR spectrometer funded by NIH Grant RR 08299 and NSF Grant BIR-9221639, and a Bruker DRX-800 NMR spectrometer funded by the Ohio Board of Regents.

* To whom correspondence should be addressed at the Department of Chemistry, The Ohio State University, 100 West 18th Avenue, Columbus, OH 43210-1173. Telephone: (614) 292-3080. FAX: (614) 292-1532. E-mail: Tsai.7@osu.edu.

[‡] Coordinates for the final ensemble of 20 structures and the NMR constraints (distance and dihedral angle constraints) have been deposited at the Brookhaven Protein Data Bank (file names 1bvm and r1bvmmr, respectively).

[§] Department of Chemistry.

^{||} Campus Chemical Instrument Center.

[⊥] Ohio State Biochemistry Program.

[#] Department of Biochemistry.

¹ Abbreviations: 1D, one-dimensional; 2D, two-dimensional; 3D, three-dimensional; COSY, correlation spectroscopy; HMQC, heteronuclear multiple-quantum coherence; HSQC, heteronuclear single-quantum coherence; ³J_{HNg}, three-bond H^N–H^α coupling constants; ³J_{Nβ}, three-bond N–H^β coupling constants; NMR, nuclear magnetic resonance; NOE, nuclear Overhauser effect; NOESY, nuclear Overhauser enhancement correlated spectroscopy; PLA2, phospholipase A₂; ppm, parts per million; RMSD, root-mean-square deviation; TOCSY, total correlation spectroscopy; WT, wild-type.

We now start a new venture—to use PLA2 and its various mutants as a system to perform in-depth structural analyses by NMR and to interpret the structural results from the functional perspective. PLA2 is small and stable, which is well suited for NMR studies. It has rich and interesting structural features (Figure 1A): a small globular protein containing six secondary structural elements (five α-helices, 1 antiparallel β-sheet), seven disulfide bonds, an Asp–His catalytic dyad, a “hydrophobic channel,” an “interfacial binding site,” and a hydrogen-bonding network. In addition, our previous studies have shown that, while PLA2 is highly stable, its conformation and stability are easily perturbed by point mutations (e.g., refs 4 and 5). The function of PLA2 is also rich and unique: it is a water-soluble protein working

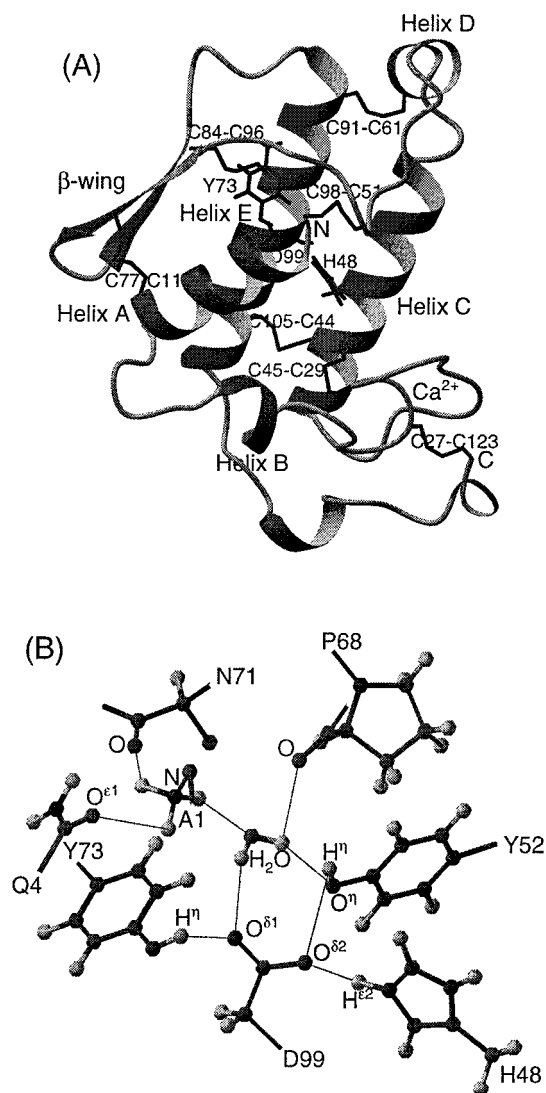


FIGURE 1: (A) Ribbon drawing of bovine pancreatic PLA2 crystal structure showing the secondary elements, seven disulfide bonds, the D99...H48 catalytic diad, and Y73 residue. The structure was taken from the Brookhaven Protein Data Bank, file PDB 1bp2.ent (10). (B) Proposed H-bonding network connects the active site residues and the interfacial site at the N-terminus (10). The figures were generated with the program MOLMOL (59).

at the surface of lipid micelles or bilayers. Furthermore, many homologous variants of PLA2 have entirely different biological functions; some of them are potent toxins or allergens. Taking advantage of such a small protein with abundant structural and functional properties, we hope to gain further insight into the structure–function relationship of PLA2 in particular and enzymes in general.

The vast majority of structural and functional analyses of pancreatic PLA2 have been performed on porcine and bovine protein. The two versions of PLA2 share ca. 85% homology in the primary sequence. While both solution (6, 7) and crystal structures (8) of porcine PLA2 have been determined, only the crystal structure of bovine PLA2 is available (9, 10). The two crystal structures are highly similar as expected. However, some notable differences were also revealed particularly in the loop region from residues 59 to 72 (8). It is essential to determine the solution structure of bovine PLA2 because all of our previous functional and mechanistic analyses have been performed on this protein.

Furthermore, the solution structure of porcine PLA2 (the only solution structure of pancreatic PLA2 available to date) was determined at an acidic pH of 4.3, while the catalytic activity of PLA2 is optimal at pH 6–8. Although many NMR structures have been determined at slightly acidic pH (which is favorable for the detection of backbone NH protons), and the global structures seem to be similar to the corresponding crystal structures in most cases, the structure at acidic pH is not suitable for detailed correlation with the mechanism and function of the enzymes, which is the primary goal of this series of papers. For PLA2, there are key aspartate residues at the active site and the Ca^{2+} -binding site. They could be partially protonated at pH 4.3, resulting in the perturbation of structural and functional properties. In fact, the solution structure of porcine PLA2 did not superimpose well with the corresponding crystal structure; the RMSD between the two structures are 2.5 Å for backbone atoms and 3.4 Å for all heavy atoms excluding the highly flexible surface loop (residues 59–72) (6). It is undoubtedly true, as the authors admitted, that some of the differences were caused by the acidic pH used in the structural determination, which inevitably dilutes the significance of their results.

This work started with three major goals: (a) determination of the solution structure of Ca^{2+} -bound bovine pancreatic PLA2 at pH 6.0 at a high resolution; (b) comparison of the solution structure of bovine PLA2 with its crystal structure; and (c) analysis of the structural features in functional terms. For the last goal, we focus on the N-terminus and the H-bonding network at present. The N-terminus is known to be intimately involved in interfacial binding (11). The H-bonding network, involving several residues in the active site and the N-terminus (Figure 1B), was thought to be important for the interfacial catalysis of PLA2 (8, 12). However, the functional role of the H-bonding network was called into question on the basis of several studies, particularly the report that the triple mutant D99N/Y52F/Y73F retains considerable catalytic activity (3).

Our results are significant in several aspects: (i) The high-resolution NMR structure, obtained at neutral pH, allowed detailed comparison with the crystal structure and revealed several notable differences. It was found that several functional sites (N-terminus, calcium-binding site, and the surface loop) appeared to be flexible with high RMSD. The possible functional implications of these findings are addressed. (ii) The H-bonding network is not as well defined as that in the crystal structure. Part of the network (the portion away from N-terminus) clearly exists in solution, as evidenced by direct observation (at 11.1 ppm) of a strong H-bond between D99 and Y73 and an implicated interaction between D99 and H48. (iii) Combining detailed NMR assignments and conformational stability data of WT PLA2 and various site-specific mutants, we have demonstrated a structural role of the H-bonding network to the extent of its existence. Specifically, the H-bond between Y73 and D99 contributes significantly (2–3 kcal/mol) to the conformational stability, whereas the D99...H48 is important for maintaining conformational integrity.

MATERIALS AND METHODS

Sample Preparation. Bovine pancreatic PLA2 was over-expressed in *E. coli* BL21(DE3)[plysS] cells. The procedures

Table 1: NMR Experiments Conducted for Structural Determination^a

experiment at pH 6.0	acquired data matrix (nucleus)			spectral width (Hz)			no. scans/FID
	t1	t2	t3	ω1	ω2	ω3	
¹ H– ¹⁵ N HSQC	256 (N)	2048 (H)		2128	9615		96
¹ H– ¹³ C HSQC	256 (C)	2048 (H)		24146	9615		4
NOESY in H ₂ O (τ _{mix} = 200 ms)	512 (H)	2048 (H)		9615	9615		72
NOESY in D ₂ O (τ _{mix} = 200 ms)	800 (H)	2048 (H)		9615	9615		72
COSY in H ₂ O	512 (H)	2048 (H)		9615	9615		80
COSY in D ₂ O	512 (H)	2048 (H)		9615	9615		80
TOCSY in H ₂ O (τ _{mix} = 35 ms)	460 (H)	2048 (H)		9615	9615		128
3D ¹ H– ¹⁵ N TOCSY–HSQC in H ₂ O (τ _{mix} = 72.1 ms)	160 (H)	64 (N)	2048 (H)	9615	2128	9615	16
3D ¹ H– ¹³ C HCCH–TOCSY in H ₂ O (τ _{mix} = 17.2 ms)	56 (C)	160 (H)	2048 (H)	3319	7183	7183	16
3D ¹ H– ¹⁵ N NOESY–HSQC in H ₂ O (τ _{mix} = 120 ms)	460 (H)	64 (N)	2048 (H)	9615	2128	9615	16
3D ¹ H– ¹³ C NOESY–HMQC in D ₂ O (τ _{mix} = 120 ms)	320 (H)	128 (C)	2048 (H)	9615	12072	9615	16
3D HNHA in H ₂ O	160 (H)	96 (N)	2048 (H)	9615	2128	9615	16
3D HNHB in H ₂ O	200 (H)	64 (N)	2048 (H)	9615	2128	9615	16
3D HNCA in H ₂ O	110 (C)	60 (N)	2048 (H)	4527	2128	9615	32
3D HN(CO)CA in H ₂ O	120 (C)	60 (N)	2048 (H)	5000	2128	6009	32
3D HNCACB in H ₂ O	90 (C)	64 (N)	2048 (H)	7847	2128	9615	32
3D CBCA(CO)NH in H ₂ O	96 (C)	60 (N)	2048 (H)	8450	2128	9615	32

^a Experiments were carried out on a Bruker DMX-600 spectrometer except ¹H–¹³C NOESY–HMQC, which was conducted on a Bruker DRX-800 spectrometer.

of protein purification have been described previously (13). The preparation of isotope-labeled samples was performed essentially in the same way except that different media were used to grow cells. For uniform labeling, the cells were grown in M9 minimal media with (¹⁵NH₄)₂SO₄ as the only nitrogen source and D-glucose-¹³C₆ as the only carbon source (14, 15). For ¹⁵N-selective labeling, the cells were grown in a synthetic rich medium with isotopically enriched amino acids such as [¹⁵N]Leu for ¹⁵N-Leu sample (14–16). The labeled samples include two uniformly labeled (¹⁵N- and ¹⁵N/¹³C-PLA2) and five specific ¹⁵N-labeled (¹⁵N-Ala, ¹⁵N-Lys, ¹⁵N-Leu, ¹⁵N-Val, and ¹⁵N-Gly PLA2) samples.

The construction and purification of the mutants used for conformational stability analyses can be found in the “Phospholipase A₂ Engineering” series: D99N (4), H48A, H48N, and H48Q (5), I9V and I9F (17), D49E (18), F22Y and F106 Y (19).

NMR Samples. Unless stated otherwise, NMR samples typically contained 1.0 mM protein in 95% H₂O/5% D₂O (referred to as “H₂O” hereafter), with 50 mM CaCl₂ and 300 mM NaCl. They were adjusted to pH 6.0 of meter reading without further correction. For ¹³C/¹⁵N-labeled samples, only 0.3 mM was used because of low yield. A nonlabeled sample of 2.0 mM was prepared in 100% D₂O as described before (5) for NOESY, TOCSY, and COSY homonuclear two-dimensional (2D) NMR experiments.

NMR Experiments. Table 1 lists the main experiments conducted for structural determination. They were carried out at 37 °C on a Bruker DMX-600 spectrometer equipped with three-axis gradients. The ¹H–¹³C NOESY–HSQC experiment recorded in H₂O was very noisy compared to the ¹⁵N-edited one, mainly because of the low concentration of the ¹³C/¹⁵N-labeled sample. Thus the sample was lyophilized after triple-resonance experiments and dissolved in D₂O. A ¹H–¹³C NOESY–HMQC experiment was performed on a Bruker DRX-800 spectrometer, showing a considerable improvement in the signal-noise ratio.

One-dimensional (1D) ¹H NMR experiments were performed at pH 6.0 in H₂O on the mutants selected for conformational stability analyses. The assignment of the ζ-OH proton of Y73 was checked by 2D NOESY experi-

ments. We have also conducted ¹H–¹⁵N HSQC and ¹H–¹⁵N NOESY–HSQC experiments on ¹⁵N-labeled H48 mutants (H48A, H48N, and H48Q), which confirmed the native-like structures of these mutants under this pH condition. The results will be reported elsewhere.

Data were processed with XWINNMR (ver. 2.0, Bruker) installed on Indigo Silicon Graphics computers. Generally, one or two times zero-filling was employed in all indirectly detected dimensions. The appropriate window function was applied on each dimension followed by Fourier transformation and baseline correction.

Proton and ¹³C chemical shifts were referenced to an internal or external 5,5-dimethylsilapentanesulfonate (DSS) standard at 0.0 ppm (20), while ¹⁵N chemical shifts were referenced to external 1.5 M (¹⁵NH₄)NO₃ in 1 M HNO₃ at 21.6 ppm (21).

Structural Calculation. Structures were calculated with restrained molecular dynamics using X-PLOR program (22) installed on Silicon Graphics O2 computers. The approach employed was ab initio simulated annealing starting from the template to explore the conformational space allowed by combinations of empirical energy functions and experimental data (23). The initial structure (random coil) used in the calculation was without the seven disulfide bonds (but with the bond distance constraints) to avoid an incorrect global fold. The resulting structures were used as the new starting points and were subjected to the second run of calculation with seven disulfide bonds fixed. The quality of the NMR structure was evaluated by RMSD. The result was gradually improved by using an iterative strategy of structure-based assignment (24).

RESULTS AND DISCUSSION

Chemical Shift Assignments and J Coupling Constants. The solution structure was determined at pH 6.0. This choice was a compromise between two considerations. Under slightly acidic conditions, higher resolution can be achieved (18, 25, 26) and more NH resonances can be observed in HSQC. However, at acidic pH, the protein may lose some calcium binding affinity as well as catalytic efficiency.

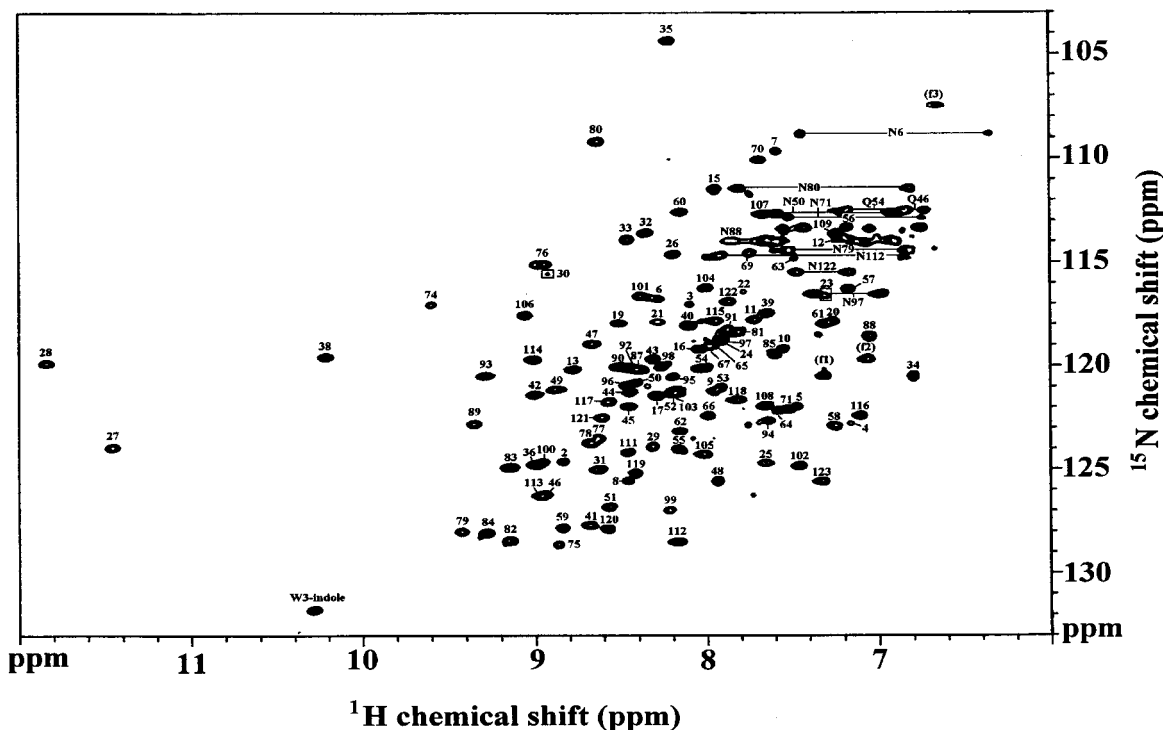


FIGURE 2: ^1H - ^{15}N HSQC spectrum of PLA2 recorded at 37 °C. The sample is 1.0 mM protein in 95% H_2O /5% D_2O with 50 mM CaCl_2 and 300 mM NaCl (pH 6.0). The cross-peaks labeled by f1, f2, and f3 are the folded peaks, which have been assigned to the amides of $\text{NH}^\epsilon(\text{R43})$, $\text{NH}^\epsilon(\text{R100})$, and $\text{NH}^\gamma(\text{R43}$ and/or $\text{R100})$, respectively.

The sequence-specific resonance assignments were carried out by identifying $d_{\text{NN}}(i, i+1)$ and $d_{\alpha\text{N}}(i, i+1)$ NOEs mainly from three-dimensional (3D) ^1H - ^{15}N NOESY-HSQC. These backbone assignments were verified by $^{13}\text{C}^\alpha/^{13}\text{C}^\beta$ chemical shifts from the following triple-resonance experiments: HNCA (27), HNCACB (28), HN(CO)CA (29), and CBCA(CO)NH (30). Specifically labeled samples and aromatic assignments (26, 31) provided assistance for the identification of amino acid type. The chemical shift assignments were completed by extending the correlation from backbone amide protons to all side chains through the following experiments: 2D COSY and TOCSY, 3D HNHA (32), 3D HNHB (33), ^1H - ^{15}N TOCSY-HSQC, and ^1H - ^{13}C HCCH-TOCSY (34). Diastereotopic protons of C^βH_2 groups were stereospecifically assigned on the basis of $^3J_{\text{N}\beta}$ information from HNHB spectra and relative magnitudes of intrasidue NOEs in NOESY spectra (35). $^3J_{\text{HN}\alpha}$ values were extracted from a quantitative analysis of the diagonal to cross-peak intensity ratio in HNHA experiment (36). Most of the NOE assignments were made on 3D ^1H - ^{15}N NOESY-HSQC and 3D ^1H - ^{13}C NOESY-HMQC spectra. However, the assignments of aromatic side chains were largely made on the basis of a 2D NOESY spectrum recorded in D_2O . Torsion angle constraints consist of backbone dihedral angle ϕ and side chain dihedral angle χ^1 . The former was derived from $^3J_{\text{HN}\alpha}$ coupling constants, and the latter was obtained from the stereospecific assignment of C^βH_2 groups.

More than 99% of H^N , H^α , and H^β , and about 90% of other side chain protons have been assigned, including stereospecific assignment on 47 C^βH_2 groups. In addition, 71 $^3J_{\text{HN}\alpha}$ constants were quantitatively determined. A ^1H - ^{15}N HSQC spectrum with assignments labeled is shown in Figure 2. Out of 119 possible backbone amides, A1, N72, and S86 remain elusive under our experimental conditions.

The total chemical shift assignments and $^3J_{\text{HN}\alpha}$ constants are provided in the Supporting Information (Supplementary Table 1).

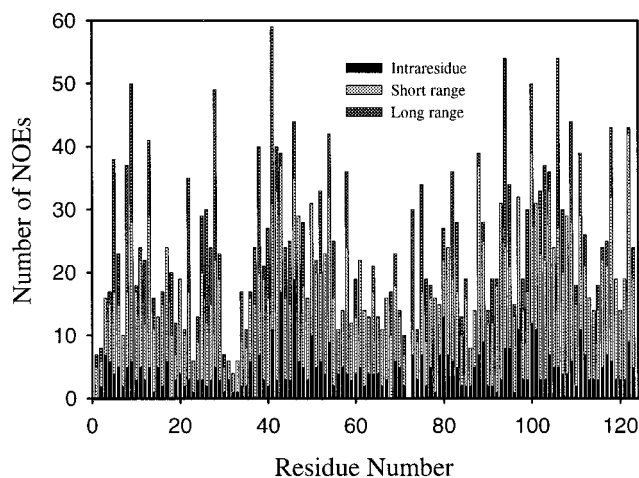
Structural Determination. The secondary structures were determined from characteristic short-range NOE patterns, ϕ scalar coupling constants ($^3J_{\text{HN}\alpha}$), and chemical shift values of $^{13}\text{C}^\alpha$ and $^{13}\text{C}^\beta$ (37, 38). Four α -helices (W3-I13; D40-L58; D59-V63; and A90-K108) and one antiparallel β -sheet (S74-S78 and E81-S85) were clearly identified. NOE intensities were classified as strong, medium, weak, and very weak, corresponding to interproton distance constraints of 1.8–2.7, 1.8–3.6, 1.8–5.0, and 1.8–6.0 Å, respectively. For unresolved NOE cross-peaks, such as methyl groups, prochiral centers, and aromatic rings, the heavy atom bound to the protons was used to assign the distance constraint with some corrections. In these cases, 1 Å was added to the upper limit for directly attached heavy atoms (e.g., C^β for C^βH_2) and 2 Å was added for a second heavy atom (e.g., C^γ for H^δ of tyrosine and phenylalanine). Dihedral angle ϕ was specified in the range of $-65^\circ \pm 30^\circ$ and $-135^\circ \pm 40^\circ$ for $^3J_{\text{HN}\alpha} < 6$ Hz and $^3J_{\text{HN}\alpha} > 8$ Hz, respectively.

A total of 1852 constraints were collected as summarized in Table 2. The distribution of NOE-derived distance restraints for each residue is displayed in Figure 3. Additional hydrogen-bond restraints (80 total) identified in the secondary elements were also added in the input for structural calculation.

Twenty good structures were selected from 40 calculation results. None of them display distance violations over 0.5 Å and dihedral angle violations over 20° . The structural statistics are listed in Table 2. Figure 4A shows the best-fit superpositions of the backbone (N, C^α , C) atoms of these 20 conformers, while Figure 4B displays the average RMSD

Table 2: Summary of Constraints and Structure Statistics for the Final 20 Structures of PLA2

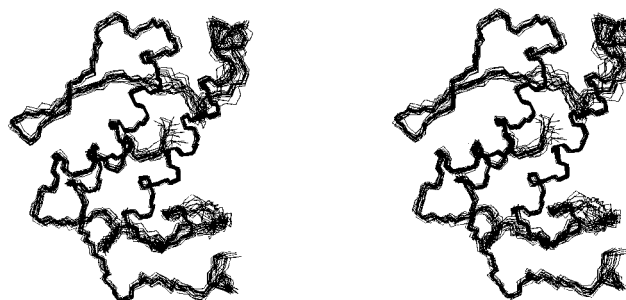
constraint (total 1934)	no.
intraresidue NOE	552
short-range NOE ($1 \leq i - j \leq 5$)	829
long-range NOE ($5 < i - j$)	360
side chain dihedral angle χ^1	58
backbone dihedral angle ϕ	53
hydrogen bond	82
RMSD	$\langle SA \rangle$
From Experimental Constraints	
NOE distance (Å)	0.00286 ± 0.00003
dihedral angles (deg)	2.4 ± 0.6
From Idealized Geometry	
bonds (Å)	0.00253 ± 0.00004
angles (deg)	0.518 ± 0.003
impropers (deg)	3.68 ± 0.03
From the Mean Structure	
backbone heavy atoms (Å)	0.62 ± 0.08
all heavy atoms (Å)	0.98 ± 0.09

FIGURE 3: NOE distribution as a function of residue number. In this figure, the NOEs are categorized as intraresidue NOE, short-range NOE ($1 \leq i - j \leq 5$), and long-range NOE ($5 < i - j$) (also see Table 2).

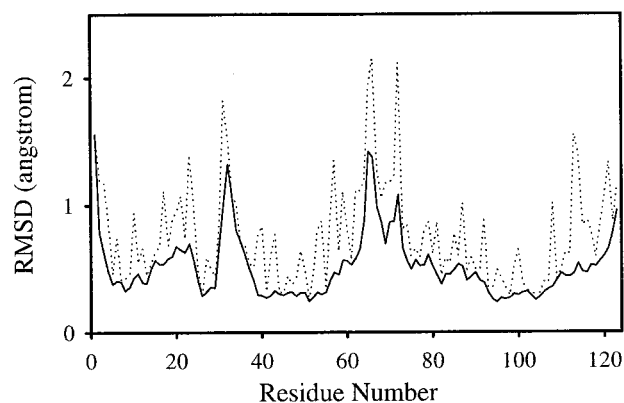
as a function of residue number. The overall RMSD is 0.62 ± 0.08 Å for backbone atoms and 0.98 ± 0.09 Å for all heavy atoms. Clearly the structure is well defined in most regions, with the exceptions of the first three N-terminal residues, the calcium-binding loop (Y25–T36), and the surface loop (V63–N72). The possible reasons and significance for these regions will be addressed in later sections.

The mean structure was subjected to further energy minimization to correct bond lengths and bond angles (22), which will be used in the following section for comparison with the crystal structure. The stereochemical quality was examined by Ramachandran plot showing the distribution of the (ϕ , ψ) angles (Supplementary Figure 1). Approximately 80% of the backbone torsion angles fall within the most favored regions, with the rest in additional allowed regions. No serious distortions were observed.

Comparison with the Crystal Structure of Bovine PLA2 and the Solution Structure of Porcine PLA2. As mentioned in the introduction, significant differences between the solution structure and the crystal structure of porcine pancreatic PLA2 have been reported, but the comparison may not be very meaningful because the solution structure was



(A)



(B)

FIGURE 4: (A) Stereoview showing the best-fit superposition of the backbone (N, C α , C) atoms of the 20 best structures generated by X-PLOR. (B) Average RMSD as a function of residue number for backbone atoms (solid line) and all heavy atoms (dotted line).

determined at pH 4.3. At this pH, the protonation states of key His and Asp residues are altered and the Ca²⁺-binding affinity may be significantly weakened. On the basis of a recent report (39), one can even question whether the reported porcine PLA2 solution structure is the Ca²⁺-bound form. Thus, our PLA2 structure reported in this paper is the first functionally relevant solution structure of PLA2.

Here we report the comparison between the solution structure and the crystal structure (with resolution of 1.7 Å, refs 9, 10) of bovine PLA2, both obtained at neutral pH in the presence of Ca²⁺. Figure 5A reveals that the backbone traces overlap very well with similar secondary elements and overall tertiary fold, whereas Figure 5B details the comparisons residue-by-residue (see ref 6 for comparison). The overall RMSD between these two structures is 1.11 Å for all backbone atoms and 1.62 Å for all heavy atoms. Apparently the agreement between our solution structure and bovine crystal structure is significantly better than the previous report for the porcine enzyme (6). In addition, both the NMR and X-ray structures of bovine PLA2 appear closer to the X-ray structure of porcine PLA2 (40) than its NMR structure (6); the RMSD values for C α atoms (residues 1–123) are 1.94 and 1.49 Å vs 2.87 and 2.68 Å, respectively. The backbone trace of the porcine solution structure is also shown in Figure 5A, which reveals large deviations in the calcium-binding loop (Figure 5B).

The differences between the solution structure of bovine PLA2 and its crystal structure are summarized as follows: the first three residues at the N-terminus are flexible in solution but assume rigid helical conformation in crystal;

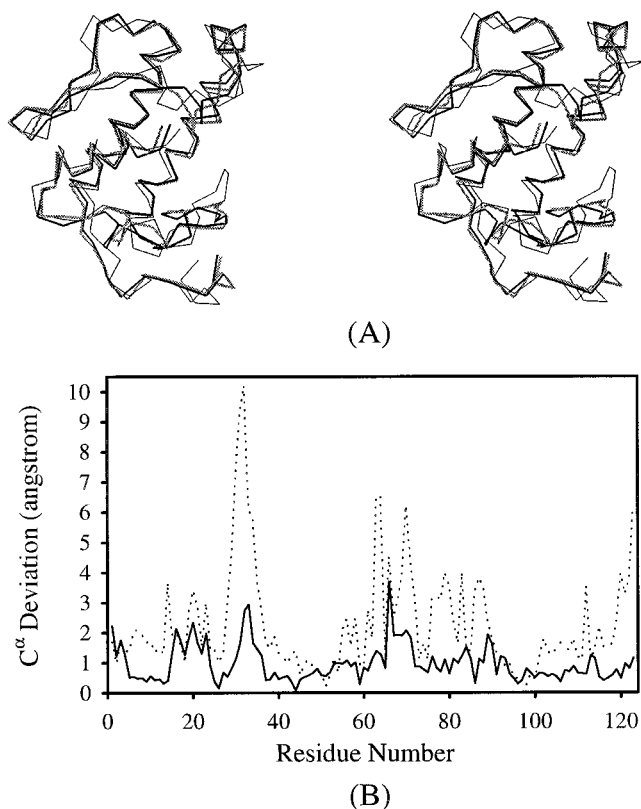


FIGURE 5: (A) Stereoview of the overlaid backbone (C^{α}) traces: bovine PLA2 solution structure (thick black line), bovine PLA2 crystal structure (thick gray line), and porcine PLA2 solution structure (thin black line, PDB filename 1pir). (B) Detailed comparisons between X-ray structure and NMR structure of bovine PLA2 (full line) and between solution structures of bovine and porcine PLA2 (dotted line): C^{α} atom deviation as a function of residue number.

the helix B (E17–F22) in the crystal structure is absent in solution; the calcium-binding loop (Y25–T36) is well-defined in crystal but displays flexibility in solution; the helix D was found to be shorter (D59–V63 instead of D59–D66) in solution; the surface loop (V63–N72) seems to be flexible; and the H-bonding network does not appear well-defined in solution. As shown in Figure 5B, there are relatively large deviations between the solution and the crystal structures in the flexible regions. Since helix B is absent in the solution structure, we label the four helices in the solution structure as helices I (W3–I13), II (D40–L58), III (D59–V63), and IV (A90–K108), which correspond to helices A, C, D, and E, respectively, in the crystal structure.

The differences between solution and crystal structures of bovine PLA2 are elaborated in the following sections, along with the discussion of their structural and functional implications. Wherever applicable, the relevance or irrelevance of the previous solution structure of the porcine enzyme at acidic pH is also addressed.

The N-Terminal Segment Is Flexible but Not Totally Disordered in Solution. The N-terminus has been suggested to play an important role in the interfacial recognition of PLA2 (11, 12). It is always observed to be helical in X-ray crystallography (41). However, in the solution structure of free porcine PLA2 (6) obtained at acidic pH, the first 3 residues at the N-terminal region were reported to be disordered. They further reported that these residues became

well defined only when the enzyme–inhibitor complex binds to lipid micelles (7). Our results for free bovine PLA2 in solution also revealed high RMSD at the N-terminus. The NOEs associated with the first several residues were typically weak and small in number. However, the N-terminus was not totally disordered. Quite a few short-range NOEs were assigned, such as $H^{\alpha}(A1)/H^{\beta}(L2)$, $H^{\beta}(A1)/H^{\beta 1}(W3)$, and $H^{\beta}(A1)/H^{\beta 1}(W3)$. More importantly, a couple of long-range NOEs have been assigned to A1 and L2, e.g., the NOE between $H^{\beta}(A1)$ and $H^{\alpha}(T70)$.

It is unclear whether the greater disordering in porcine PLA2 is the result of acidic pH or is due to the intrinsic differences between these two versions of PLA2. Nonetheless, we agree that the N-terminus in pancreatic PLA2 is less ordered in solution than in the crystal structure. The crystal-packing force probably helps the ordering in the latter form. It could also be true that the N-terminus could become more ordered when the enzyme binds to the interface and the substrate (7, 42). In fact, some conformational changes have been reported on bovine PLA2 upon micelle binding (43). It is possible that the crystal structure is closer to the E^* form (enzyme at the surface).

Helix B (E17–F22) Is Absent and Helix D (D59–D66) Is Less Stable in Solution. These two helices are well-defined in the crystal structure. For helix B, there is some evidence against the existence of α -helical conformation in the solution structure. For instance, the $^3J_{HN\alpha}$ of L20 is above 7 Hz. Furthermore, a medium NOE was observed between $H^{\alpha}(L19)$ and $H^{\beta}(D23)$ instead of between $H^{\alpha}(L19)$ and $H^{\beta}(F22)$, apparently contradicting the NOE pattern in an α -helical conformation. For helix D, the first several residues (D59–V63) appear in an α -helical conformation. The evidence includes an $\alpha\beta(i, i+3)$ NOE between D59 and K62. However, the $^3J_{HN\alpha}$ values of L64 and D66 are both close to 7 Hz, which is indicative of irregular secondary structure.

L19 and L20 in helix B were suggested to be in the putative interfacial binding site (44) and have been investigated by site-directed mutagenesis (45). In the NMR structure, these two residues together with N-terminus and several other residues still form a flat surface, the interfacial binding site. However, unlike the crystal structure, helix B and the N-terminus do not assume rigid α -helical conformation. One possible consequence of this picture is that the interfacial binding site is more flexible than what was shown by the crystal structure.

The helix D does not exist in an α -helical structure in either the crystal or the solution structure of porcine PLA2 (8). The different behavior in this segment between bovine and porcine PLA2 was attributed to one residue difference (V63 in bovine vs F63 in porcine) in the otherwise invariant segment (46).

The Surface Loop Is More Flexible in Solution. We show that the high RMSD in the surface loop (V63–N72) is caused by intrinsic problems (conformational flexibility and/or conformational heterogeneity) rather than by incomplete data analysis. Table 3 lists the 1H and ^{13}C chemical shifts of methyl groups in four valine residues. Clearly, V63 and V65 have the values close to those in random coils. Seeking more evidence, we performed the $^3J_{C\gamma CO}$ experiment (47) on the ^{13}C , ^{15}N -labeled PLA2 (Table 3). The results of T36, V38, T47, T83, V109, and five isoleucine residues are consistent with the χ^1 torsion angles inferred from HNHB and NOE

Table 3: Chemical Shifts, ³J_{C_γCO} Coupling Constants, and the χ¹ Values of Val, Thr, and Ile Residues

residue	chemical shift (ppm) ^a	³ J _{C_γCO} (Hz) ^b	χ ¹ from HNHB and NOESY
V38	C ^{γ1} = 22.4; H ^{γ1} = 0.83	γ1: 3.2	-60°
	C ^{γ2} = 18.5; H ^{γ2} = 0.42	γ2: 1.0	
V63 ^c	C ^{γ1} = 21.4; H ^{γ1} = 0.97	γa: 1.3	rotamer averaging?
	C ^{γ2} = 20.4; H ^{γ2} = 0.97	γb: 1.7	
V65 ^c	C ^{γ1} = 21.7; H ^{γ1} = 0.89	γa: 1.9	rotamer averaging?
	C ^{γ2} = 21.2; H ^{γ2} = 0.91	γb: < 1.0	
V109	C ^{γ1} = 22.3; H ^{γ1} = 1.02	γ1: 3.3	-60°
	C ^{γ2} = 18.4; H ^{γ2} = 1.02	γ2 < 1.0	
T36	C ^{γ2} = 21.3; H ^{γ2} = 1.32	<1.0	-60°
T47	C ^{γ2} = 22.5; H ^{γ2} = 1.25	<1.0	-60°
T70	C ^{γ2} = 21.8; H ^{γ2} = 1.23	2.3	rotamer averaging?
T83	C ^{γ2} = 21.4; H ^{γ2} = 1.11	<1.0	-60°
I9	C ^{γ2} = 18.8; H ^{γ2} = 0.67	<1.0	-60°
I13	C ^{γ2} = 19.7; H ^{γ2} = 0.89	<1.0	-60°
I82	C ^{γ2} = 18.1; H ^{γ2} = 1.05	<1.0	-60°
I95	C ^{γ2} = 18.2; H ^{γ2} = 0.90	<1.0	-60°
I104	C ^{γ2} = 17.4; H ^{γ2} = 0.87	<1.0	-60°

^a The uncertainties are estimated to be 0.05 ppm and 0.2 ppm for ¹H and ¹³C, respectively. ^b The uncertainty is estimated to be 0.2 Hz. ^c The stereospecific assignment was tentative.

data, but the χ¹ angles of V63, V65, and T70 could not be assigned. In this *J* experiment, these three residues appear to have averaged *J* coupling constants, indicating that they are likely to have rotamer averaging.

The surface loop is part of the interfacial recognition face of PLA₂. Because the surface loop is well defined in the crystal structure of bovine PLA₂ but mobile in the crystal structure of *pro*-PLA₂, it has been suggested that rigidity of the surface loop is required for effective interfacial binding (11). This result and the result of the N-terminus residues taken together suggest that there are significant conformational differences between solution and crystal structures and that these differences are reminiscent of those between E (free enzyme in solution) and E* (enzyme bound to the interface) forms. This concept challenges the suggestion from X-ray analyses that there are few conformational changes between the E and E* forms (48). There is growing evidence that the changes are recognizable and could be important between E and E* forms in PLA₂ (6, 7, 42, 43).

The Calcium-Binding Loop Is Less Defined in Solution. While the crystal structure clearly shows that Y28, G30, G32, and D49 are involved in calcium binding, the calcium ion was not included in the calculation of the solution structure because no constraints involving calcium can be obtained in the NMR study. This could be the main reason that the residues in the calcium-binding loop exhibit high RMSD values in the NMR structure (6). Another possible reason for the apparent flexibility of this segment in solution could be that the calcium ion undergoes rapid association/dissociation. The less-defined calcium-binding loop is also responsible for the relatively high RMSD in the C-terminus, which is linked through the C27–C123 disulfide bond.

Integrity of the H-Bonding Network in Solution. It was suggested that the H-bonding network, which is well demonstrated in crystal structures, exists only partially in the solution structure of free porcine pancreatic PLA₂ (6). The H-bonding network in our structure, as shown in Figure 6, appears better defined than that in the solution structure of porcine PLA₂, though not as well defined as that in the

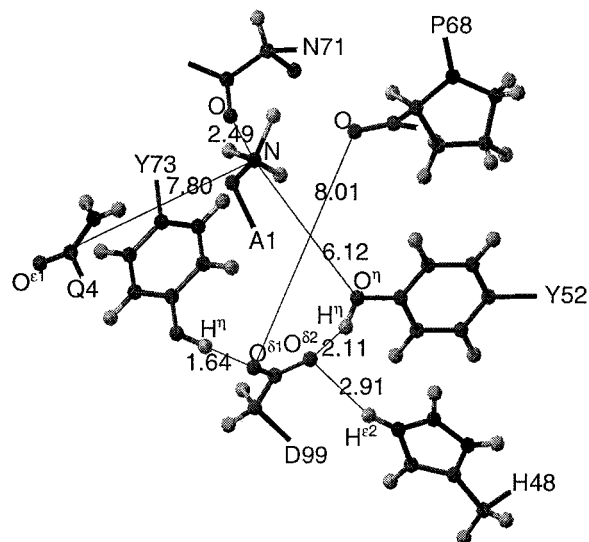


FIGURE 6: The corresponding “H-bonding network” in the minimized average structure. Overall it is not as well defined as that in the crystal structure. For instance, the distance of 7.80 Å between O^{δ1}(Q4) and N(A1) precludes a possible H-bond between these two atoms. The figure was generated with the program MOLMOL (59).

crystal structure. This is evidenced by the following observations: (1) The distance of 7.80 Å between O^{δ1}(Q4) and N(A1) in the minimized average structure (2.87 Å in the crystal structure) precludes a possible H-bond between these two atoms. (2) The distance of 8.01 Å between O(P68) and O^{δ1}(D99) is more than 2 Å longer than the corresponding distance in bovine crystal structure (5.79 Å in the crystal structure). (3) The resonances of H^{ε2}(H48), α-NH₃⁺(A1), and H^γ(Y52) could not be assigned despite extensive search, which means they could be very weak or simply absent. On the other hand, most of the other hydrogen bonds appear possible as judged by the dimensions marked in Figure 6. More importantly, we have clearly detected the Y73···D99 hydrogen bond and obtained the evidence for the implicated D99···H48 interaction as described below.

Suggestions of H-bonds in X-ray or NMR structures of proteins are usually based on distances. Direct observation is not possible in the X-ray structure and is very difficult in the NMR structure. However, we have clearly identified the H-bonding between D99 and Y73. In the 2D NOESY experiment performed in H₂O, the ¹H diagonal peak at 11.1 ppm was unambiguously assigned to phenolic hydroxyl group of Y73 based on strong NOE to H^ε and medium NOE to H^δ of Y73 (Figure 7). The proton also has strong NOEs to both H^β and weak NOEs to H^α and H^N of D99, indicating close proximity of these two residues. These assignments strongly suggest hydrogen bonding between the carboxylic side chain of D99 and the phenolic hydroxyl group of Y73.

The Y73···D99 interaction can be further extended to a three-residue stretch, Y73···D99···H48. As also shown in Figure 8, the 11.1 ppm peak is clearly present in H48Q but is absent in H48N and H48A, suggesting that the Y73···D99 hydrogen bond is perturbed when the D99···H48 hydrogen bond is disrupted. This result is consistent with our previous prediction (5) that the amide nitrogen atom of Gln (but not of Asn) mimics the ε₂-nitrogen of H48 and interacts with D99 through a hydrogen bond in H48Q. Disruption of this H-bonding in H48N or H48A disrupts the “network” and leads to the disruption of the Y73···D99

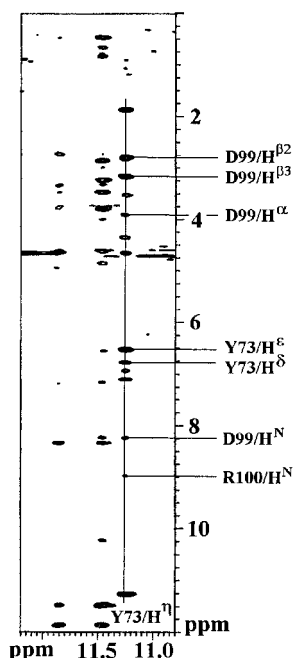


FIGURE 7: Downfield region of the 2D NOESY spectrum recorded in H₂O shows the important NOE assignments for H^γ(Y73), suggesting an H-bond between the phenolic hydroxyl group of Y73 and carboxylic side chain of D99.

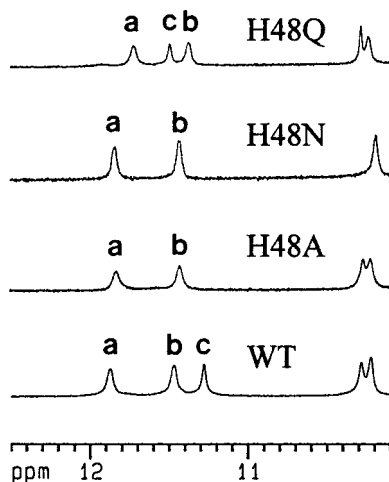


FIGURE 8: Downfield region of 1D ¹H NMR spectra of H48 mutants recorded at 37 °C. The samples contained 0.7 mM protein in 95% H₂O/5% D₂O with 50 mM CaCl₂ and 300 mM NaCl (pH 6.0). The spectrum of WT PLA2 is also shown for comparison. The peaks marked with a, b, and c correspond to the resonances of H^N(Y28), H^N(C27), and H^γ(Y73), respectively.

hydrogen bond. The crystal structure of H48Q, which has just been completed, strongly supports this interpretation (49).

What Is the Role of the Hydrogen-Bonding Network? The H-bonding network, which links the active site to the interfacial recognition site, was suggested to be important for the interfacial catalysis of PLA2 (8, 12). This proposition has been easily questioned by the demonstration that deletion of the phenolic OH group of Y73 did not affect the catalytic activity of PLA2 (25). Moreover, we have constructed single, double, and even triple mutants on the most conserved residues of Y52, Y73, and D99 in the H-bonding network. These mutants have been investigated by scooting-mode kinetics and X-ray crystallography (3, 25, 49–52). In the Y52F/Y73F/D99N triple mutant, kinetic analysis demon-

strated retention of considerable activity (with a k_{cat} value of 5% compared to WT), while the X-ray crystal structure revealed a substantial disruption of the H-bonding network (3). Thus the mounting evidence suggests that the so-called H-bonding network is *not* crucial for any form of interfacial activation and the effect on catalytic function is modest at best.

We suggest that the H-bonding network in bovine PLA2 (to the extent of its existence) is of structural importance on the basis of the analyses of a series of mutants. In the following sections we show that the Y73···D99 hydrogen bond may contribute significantly to the conformational stability of PLA2, whereas D99···H48 may help to maintain the structural integrity.

The Y73···D99 H-Bond May Contribute Significantly to Conformational Stability. Although it is a general perception that hydrogen bonds contribute to the conformational stability of proteins, quantitative analysis has been difficult because proteins contain hundreds or thousands of hydrogen bonds but are only marginally stable. The free energy of unfolding, $\Delta G_d^{H_2O}$, falls in the range 5–15 kcal/mol for most proteins. The conformational stability for WT PLA2 is 9.5 kcal/mol; those of the mutants D99A, Y73F, Y73A, and Y73F/Y52F double mutant are 4.6, 5.3, 4.8, and 4.1 kcal/mol, respectively (25, 53). Because the Y73···D99 H-bond is definitely missing in these mutants, one might say that this H-bond contributes ca. 5 kcal/mol to the conformational stability of PLA2. This reasoning, though commonly employed, is highly oversimplified, since there is no experimental evidence that the net structural difference between these mutants and WT PLA2 is a single hydrogen bond (54). One can easily counter that at least two hydrogen bonds should be missing in the Y73F/Y52F double mutant. In fact, we have obtained the crystal structure of this double mutant, which indicates that four hydrogen bonds around the mutation sites are missing, but hydrophobic interactions have been enhanced (51).

Three more mutants Y73S, Y73K, and D99N have been constructed on Y73 and D99 residues. The D99N is the only mutant that has the possibility to form a Y73···N99 H-bond similar to that of WT and thus retain similar stability. However, 1D ¹H NMR revealed the absence of Y73 hydroxyl group resonance in the downfield region. The X-ray structure also revealed that the carbonyl oxygen of N99 side chain pointed toward the H48 imidazole ring (52). Thus, there is no evidence of this H-bond in D99N. The conformational stability of these three mutants was measured to be 5.3, 4.6, and 4.7 kcal/mol, respectively, which are lower than that of WT by 4–5 kcal/mol.

We further examined several other site-specific mutants where the site of mutation is unrelated to Y73 or D99. Surprisingly, the correlation between the Y73···D99 hydrogen bond and the conformational stability seems to hold: for the five mutants (I9V, F22Y, H48Q, D49E, and F106Y) displaying WT-like stability, the 11 ppm resonance is retained; for the three mutants (I9F, H48N, and H48A) with decreased stability ($\Delta G_d^{H_2O} = 7.5, 6.5,$ and 6.4 kcal/mol, respectively), the 11 ppm resonance is lost. The correlation is particularly noteworthy for H48N, H48A, and H48Q (9.6 kcal/mol). These analyses suggest that the Y73···D99 hydrogen bond contributes significantly (up to 2–3 kcal/mol) to the conformational stability of PLA2. This number is relatively high compared to the value of 1–2 kcal/mol

reported by Myers and Pace (55, 56) for the net stabilization of proteins by hydrogen bonds, as well as the value of 2 kcal/mol reported for lysozyme (57).

The changes in stability in general cannot be equated directly with the absolute values of the interaction energy (D99•••Y73 in our work) (58). However, it is possible that this hydrogen bond is relatively strong, as indicated by the higher deshielding of the Y73 hydroxyl proton compared to other reports (http://bmr.wis.edu/ref_info/ref_info.html). Close examination of the PLA2 structure suggests that the Y73•••D99 hydrogen bond is probably the only stabilizing force between helix IV and the unanchored β -segment S74–S78.

D99•••H48 Catalytic Dyad Helps to Maintain Structural Integrity. The D99•••H48 dyad is the key catalytic machinery, but it is also part of the H-bonding network and contributes to the conformational integrity as demonstrated in H48 mutants.

There are two possible structural roles for the D99•••H48 H-bond. One is evident that the interaction helps to orient the proper tautomeric form of the imidazole ring required for proper enzymatic function. The other is that it anchors the D99 carboxylate side chain to ensure the correct formation of the Y73•••D99 hydrogen bond, which has been shown in this work to contribute significantly to the enzyme stability. Our previous functional analyses suggested that H48N retains part of the first role, whereas H48Q retains part of the second role (5). The results in Figure 8 support this interpretation.

The D99•••H48 interaction could also help to stabilize the two major helices, helix II (D40–L58) and helix IV (A90–K108), cross-linked by two disulfide bonds (C44–C105 and C51–C98). Hydrogen–deuterium exchange experiments indicated that helix IV is the most stable secondary element in this protein, followed by helix II. After 3 h in D₂O, the following 17 NH peaks were still present in the ¹H–¹⁵N HSQC experiment: D42, H48, C51, A93, I95, C96, N97, C98, D99, R100, N101, A102, A103, I104, C105, F106, and S107. After 6 days, the following NH protons could still be detected: C96, N97, C98, D99, R100, N101, A102, A103, I104, and F106.

In conclusion, we have solved the solution structure of bovine pancreatic PLA2 at a functionally relevant pH. The structure agrees with the bovine crystal structure globally, but also reveals important differences. The solution structure, as well as its differences from the crystal structure, has been analyzed in detail and in relation to the catalytic events. The in-depth structural analyses of WT PLA2 presented in this paper will permit detailed structural and dynamic studies of various PLA2 mutants. One such study, the characterization of a molten globule-like state, is presented in the following paper (60).

ACKNOWLEDGMENT

The authors gratefully acknowledge Dr. B. Volkman at NMRFAM for providing the HNHB pulse sequence.

SUPPORTING INFORMATION AVAILABLE

One table containing the ¹H, ¹⁵N, and ¹³C resonance assignments and ³J_{HN α constants (Supplementary Table 1) and one figure of the Ramachandran plot for the minimized}

average solution structure (Supplementary Figure 1). This material is available free of charge via the Internet at <http://pubs.acs.org>.

REFERENCES

- Dennis, E. A. (1994) *J. Biol. Chem.* 269, 13057–13060.
- Dennis, E. A. (1997) *Trends Biochem. Sci.* 22, 1–2.
- Sekar, K., Yu, B.-Z., Rodgers, J., Lutton, J., Liu, X.-H., Chen, X., Tsai, M.-D., Jain, M. K., and Sundaralingam, M. (1997) *Biochemistry* 36, 3104–3114.
- Dupureur, C. M., Li, Y., and Tsai, M.-D. (1992) *J. Am. Chem. Soc.* 114, 2748–2749.
- Li, Y., and Tsai, M.-D. (1993) *J. Am. Chem. Soc.* 115, 8523–8526.
- van den Berg, B., Tessari, M., de Haas, G. H., Verheij, H. M., Boelens, R., and Kaptein, R. (1995) *EMBO J.* 14, 4123–4131.
- van den Berg, B., Tessari, M., Boelens, R., Dijkman, R., Kaptein, R., de Haas, G. H., and Verheij, H. M. (1995) *J. Biomol. NMR* 5, 110–121.
- Dijkstra, B. W., Renetseder, R., Kalk, K. H., Hol, W. G. J., and Drenth, J. (1983) *J. Mol. Biol.* 168, 163–179.
- Dijkstra, B. W., Drenth, J., Kalk, K. H., and Vandermaelen, P. J. (1978) *J. Mol. Biol.* 124, 53–60.
- Dijkstra, B. W., Kalk, K. H., Hol, W. G., and Drenth, J. (1981) *J. Mol. Biol.* 147, 97–123.
- Dijkstra, B. W., Kalk, K. H., Drenth, J., de Haas, G. H., Egmond, M., and Slotboom, A. J. (1984) *Biochemistry* 23, 2759–2766.
- Verheij, H. M., Slotboom, A. J., and de Haas, G. H. (1981) *Rev. Physiol. Biochem. Pharmacol.* 91, 91–203.
- Noel, J. P., Bingman, C. A., Deng, T., Dupureur, C. M., Hamilton, K. J., Jiang, R.-T., Kwak, J.-G., Sekharudu, Y. C., Sundaralingam, M., Tsai, M.-D. (1991) *Biochemistry* 30, 11801–11811.
- Muchmore, D. C., McIntosh, L. P., Russel, C. B., Anderson, D. E., and Dahlquist, F. W. (1989) *Methods Enzymol.* 177, 44–73.
- Li, Y. (1994) Ph.D. Dissertation, The Ohio State University, Columbus, OH.
- Pelton, J. G., Torchia, D. A., MeAdow, N. D., Wong, C.-Y., and Roseman, S. (1991) *Biochemistry* 30, 10043–10057.
- Liu, X., Zhu, H., Huang, B., Rogers, J., Yu, B.-Z., Kumar, A., Jain, M. K., Sundaralingam, M., and Tsai, M.-D. (1995) *Biochemistry* 34, 7322–7334.
- Li, Y., Yu, B.-Z., Zhu, H.-X., Jain, M., and Tsai, M.-D. (1994) *Biochemistry* 33, 14714–14722.
- Dupureur, C. M., Yu, B.-Z., Mamone, A., Jain, M. K., and Tsai, M.-D. (1992) *Biochemistry* 31, 10576–10583.
- Wishart, D. S., Bigam, C. G., Holm, A., Hodges, R. S., and Sykes, B. D. (1995) *J. Biomol. NMR* 5, 67–81.
- Srinivasan P. R., and Lichter, R. L. (1977) *J. Magn. Reson.* 28, 227–234.
- Brünger, A. T. (1992) *X-PLOR: A System for X-ray Crystallography and NMR*, Yale University Press, New Haven, CT.
- Nilges, M., Clore, G. M., and Gronenborn, A. M. (1988) *FEBS Lett.* 239, 129–136.
- Nilges, M. (1996) *Curr. Opin. Struct. Biol.* 6, 617–623.
- Dupureur, C. M., Yu, B.-Z., Jain, M. K., Noel, J. P., Deng, T., Li, Y., Byeon, I.-J., and Tsai, M.-D. (1992) *Biochemistry* 31, 6402–6413.
- Fisher, J., Primrose, W. U., Roberts, G. C. K., Dekker, N., Boelens, R., Kaptein, R., Slotboom, A. J. (1989) *Biochemistry* 28, 5939–5946.
- Grzesiek, S., and Bax, A. (1992) *J. Magn. Reson.* 96, 432–440.
- Muhandiram, D. R., and Kay, L. E. (1994) *J. Magn. Reson. B* 103, 203–216.
- Bax, A., and Ikura, M. (1991) *J. Biomol. NMR* 1, 99–104.
- Grzesiek, S., and Bax, A. (1992) *J. Am. Chem. Soc.* 114, 6291–6293.
- Zhu, H.-X., Dupureur, C. M., Zhang, X., and Tsai, M.-D. (1995) *Biochemistry* 34, 15307–15314.

32. Vuister, G. W., and Bax, A. (1993) *J. Am. Chem. Soc.* **115**, 7772–7777.
33. Archer, J. S., Ikura, M., Torchia, D. A., and Bax, A. (1991) *J. Magn. Reson.* **95**, 636–641.
34. Kay, L. E., Xu, G.-Y., Singer, A. U., Muhandiram, D. R., and Forman-Kay, J. D. (1993) *J. Magn. Reson. B* **101**, 333–337.
35. Case, D. A., Dyson, C. H., and Wright, P. E. (1994) *Methods Enzymol.* **239**, 392–416.
36. Kuboniwa, H., Grzesiek, S., Delaglio, F., and Bax, A. (1994) *J. Biomol. NMR* **4**, 871–878.
37. Wüthrich, K. (1986) *NMR of Proteins and Nucleic Acids*, Wiley & Sons, New York.
38. Spera, S., and Bax, A. (1991) *J. Am. Chem. Soc.* **113**, 5490–5492.
39. Fujii, S., Meida, M., Tani, T., Inoue, S., Iwama, S., Katsumura, S., and Ikeda, K. (1998) *Arch. Biochem. Biophys.* **354**, 73–82.
40. Finzel, B. C., Ohlendorf, D. H., Weber, P. C., and Salemme, F. R. (1991) *Acta Crystallogr. B* **47**, 558–559.
41. Arni, R. K., and Ward, R. J. (1996) *Toxicon* **34**, 827–841.
42. van den Berg, B., Tessari, M., Boelens, R., Dijkman, R., de Haas, G. H., Kaptein, R., and Verheij, H. M. (1995) *Nature Struct. Biol.* **2**, 402–406.
43. Kilby, P. M., Primrose, W. U., and Roberts, G. C. K. (1995) *Biochem. J.* **30**, 935–944.
44. Dijkstra, B. W., Drenth, J., and Kalk, K. H. (1981) *Nature* **289**, 604–606.
45. Lee, B.-I., Yoon, E. T., and Cho, W. (1996) *Biochemistry* **35**, 4231–4240.
46. Thunnissen, M. M., Franken, P. A., de Haas, G. H., Drenth, J., Kalk, K. H., Verheij, H. M., and Dijkstra, B. W. (1993) *J. Mol. Biol.* **232**, 839–855.
47. Grzesiek, S., Vuister, G. W., and Bax, A. (1993) *J. Biomol. NMR* **3**, 487–493.
48. Scott, D. L., White, S. P., Otwinoski, Z., Yuan, K., Gelb, M. H., and Sigler, P. B. (1990) *Science* **250**, 1541–1546.
49. Sekar, K., Biswas, R., Li, Y., Tsai, M.-D., and Sundaralingam, M. (1999) *Acta Crystallogr., Sect. D* **55**, 443–447.
50. Dupureur, C. M., Deng, T., Kwak, J.-G., Noel, J. P., and Tsai, M.-D. (1990) *J. Am. Chem. Soc.* **114**, 2748–2749.
51. Sekharudu, C., Ramakrishnan, B., Huang, B.-H., Jiang, R.-T., Dupureur, C. M., Tsai, M.-D., and Sundaralingam, M. (1992) *Protein Sci.* **1**, 1585–1594.
52. Kumar, A., Sekharudu, C., Ramakrishnan, B., Dupureur, C. M., Zhu, H.-X., Tsai, M.-D., and Sundaralingam, M. (1994) *Protein Sci.* **3**, 2082–2088.
53. Dupureur, C. M. (1992) Ph.D. Thesis, The Ohio State University, Columbus, OH.
54. Honig, B., and Yang, A.-S. (1995) *Adv. Protein Chem.* **46**, 27–58.
55. Myers, J. K., and Pace, C. N. (1996) *Biophys. J.* **71**, 2033–2039.
56. Pace, C. N. (1995) *Methods Enzymol.* **259**, 538–554.
57. Yamagata, Y., Kubota, M., Sumikawa, Y., Funahashi, J., Takano, K., Fujii, S., and Yutani, K. (1998) *Biochemistry* **37**, 9355–9362.
58. Fersht, A. R., and Serrano, L. (1993) *Curr. Opin. Struct. Biol.* **3**, 75–83.
59. Koradi, R., Billeter, M., and Wüthrich, K. (1996) *J. Mol. Graphics* **14**, 51–55.
60. Yuan, C.-H., Byeon, I.-J. L., Poi, M. J., and Tsai, M.-D. (1999) *Biochemistry* **38**, 2919–2929.

BI982211A